Nonlinear Dyn (2018) 93:1681–1693
https://doi.org/10.1007/s11071-018-4284-0

ORIGINAL PAPER

Dynamics of a physical SBT memristor-based Wien-bridge circuit

Mei Guo · Zhenhao Gao · Youbao Xue · Gang Dou · Yuxia Li

Received: 7 December 2017 / Accepted: 5 April 2018 / Published online: 24 April 2018

Abstract In this paper, a physical SBT memristor-based Wien-bridge chaotic circuit is proposed. The equilibrium point and stability of the chaotic circuit are analyzed theoretically. The dynamical characteristics of circuit system with the variation in the initial state and the circuit element parameters are investigated by means of Lyapunov exponents, bifurcation diagrams and phase portraits. The results show that the circuit system exhibits complex dynamic behaviors, such as stable point, period, and chaos. Specifically, the system can generate hidden chaotic attractors and coexisting chaotic attractors. All the results provide an important theoretical basis for the next physical implementation of the chaotic circuit.

Keywords Physical SBT memristor · Wien-bridge circuit · Chaos · Hidden attractors · Coexisting attractors

1 Introduction

In 2016, researchers at North Carolina State University have developed nonlinear chaos-based integrated circuits, which enable computer chips to perform multiple functions with fewer transistors [1]. As the researchers say: “The potential of 100 morphable nonlinear chaos-based circuits doing work equivalent to 100 thousand circuits, or of 100 million transistors doing work equivalent to three billion transistors holds promise for extending Moore’s law-not through doubling the number of transistors every 2 years but through increasing what transistors are capable of when combined in nonlinear and chaotic circuit” [2]. Consequently, constructing chaotic circuits is still a research hotspot.

It is well known that a nonlinear two-terminal electronic element is easily used to construct chaotic circuits. Coincidentally, the memristor is a nonlinear two-terminal electronic element revealing the relationship between magnetic flux φ and charge q [3,4], which is very suitable for designing chaotic circuits in theory. Therefore, memristor-based chaotic circuits and their generating complex dynamical behaviors have been studied extensively [5–17]. In the published studies, those existing memristors in the memristor-based chaotic circuits were mainly memristor emulators. In 2008, the first physical TiO_2-based nanostructured memristor was prepared by researchers of Hewlett–Packard Laboratory [18], which rekindled the attention of researchers to the memristor because of its potential applications in nonvolatile memory and artificial neural network [19–24]. From then on, many new material systems have been reported toward the physical memristor [25–31]. However, the physical memristor

M. Guo · Z. Gao · Y. Xue · G. Dou (✉) · Y. Li (✉)
College of Electrical Engineering and Automation, Shandong University of Science and Technology, Tsingtao 266590, People’s Republic of China
e-mail: dougang521@163.com

Y. Li
e-mail: yuxiali2004@vip.163.com

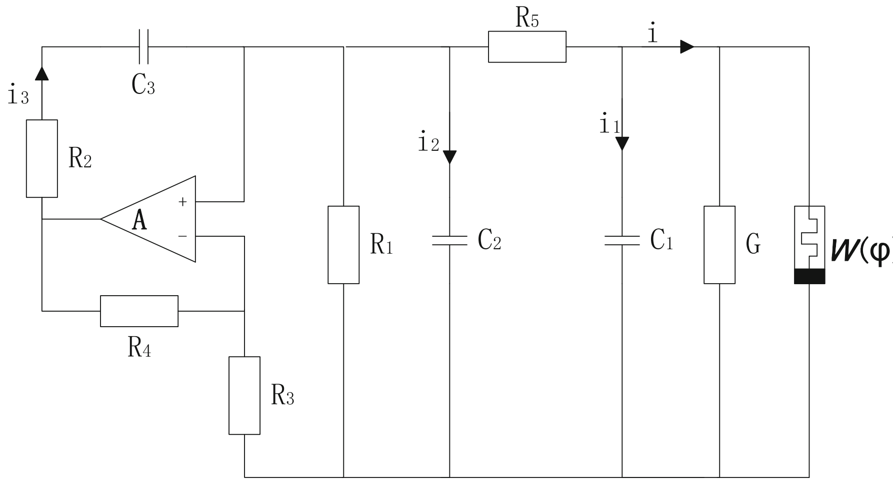

Fig. 1 The SBT memristor-based Wien-bridge chaotic circuit

is not applied into the chaotic circuit design and realization, because it is unavailable as a commercial element now.

In order to apply the physical memristor into nonlinear circuit designs, firstly, a $Sr_{0.95}Ba_{0.05}TiO_3$ (SBT) nanometer film was prepared in our laboratory [32], and then a flux-controlled mathematical model with definite parameters was established [33]. In this paper, a physical SBT memristor-based Wien-bridge chaotic circuit is proposed, and its dynamic behaviors are analyzed by means of Lyapunov exponents [34–36], bifurcation diagrams and phase portraits. It can guide the research on the realization of physical SBT memristor-based chaotic circuit in the future.

This paper is organized as follows: Sect. 2 gives a flux-controlled mathematical model of the physical SBT memristor and the physical SBT memristor-based Wien-bridge circuit. In Sect. 3, the circuit system is modeled by fourth-order state equations, the system's stability is analyzed, and the dynamics of dependence on the initial states are studied by means of numerical simulations. In Sect. 4, the impacts of circuit parameters on the dynamic behaviors of the circuit system are investigated. Finally, the conclusions are given in Sect. 5.

2 The physical SBT memristor-based Wien-bridge chaotic circuit

In our previous work, a $Sr_{0.95}Ba_{0.05}TiO_3$ (SBT) nanometer film was prepared, which can be used as a physical memristive element [32]. And the SBT memristor's flux-controlled mathematical model with deterministic parameters was obtained as follows:

$$\begin{cases} i(t) = (A + B|\varphi(t)|)u(t) \\ \frac{\mathrm{d}\varphi(t)}{\mathrm{d}t} = u(t) \end{cases}$$

where $A = 0.0676\,\mathrm{S}$, and $B = 0.3682\,\mathrm{S/Wb}$ [33]. Herein, the physical SBT memristor can be used to design chaotic circuit.

The physical SBT memristor-based Wien-bridge chaotic circuit is shown in Fig. 1. The chaotic circuit consists of an operational amplifier, three linear capacitors C_1, C_2, and C_3, five linear resistors R_1, R_2, R_3, R_4, and R_5, a linear negative conductance G, and a nonlinear physical SBT memristor. The physical SBT memristor is a fundamental circuit element, along with the resistor, capacitor and inductor, which is not composed of simulated circuit.

3 Dynamic analysis of the physical SBT memristor-based Wien-bridge circuit

3.1 Modeling of a physical SBT memristor-based Wien-bridge circuit

There are four state variables of $u_1(t)$, $u_2(t)$, $u_3(t)$ and $\varphi(t)$, which represent the voltage of the capacitor C_1, the voltage of the capacitor C_2, the voltage of the capacitor C_3, and the magnetic flux of the physical SBT memristor, respectively. The dynamical equations of the physical SBT memristor-based Wien-bridge circuit are as follows:

Table 1 The element parameter values of the physical SBT memristor-based Wien-bridge circuit

Parameters	Values
Capacitance C_1	10 nF
Capacitance C_2	20 nF
Capacitance C_3	20 nF
Resistance R_1	25 kΩ
Resistance R_2	25 kΩ
Resistance R_3	4 kΩ
Resistance R_4	10 kΩ
Resistance R_5	45 kΩ
Negative conductance G	− 0.0677 S
The A and B of SBT memristor	0.0676 S, 0.3682 S/Wb

$$\begin{cases} \frac{du_1(t)}{dt} = \frac{1}{C_1}\left(\frac{u_2(t)-u_1(t)}{R_5} - (A+B|\varphi(t)|+G)\,u_1(t)\right) \\ \frac{du_2(t)}{dt} = \frac{1}{C_2}(\frac{R_4}{R_2R_3}u_2(t) - \frac{1}{R_2}u_3(t) - \frac{1}{R_1}u_2(t) - \frac{u_2(t)-u_1(t)}{R_5}) \\ \frac{du_3(t)}{dt} = \frac{1}{C_3}(\frac{R_4}{R_2R_3}u_2(t) - \frac{1}{R_2}u_3(t)) \\ \frac{d\varphi(t)}{dt} = u_1\,(t) \end{cases} \tag{1}$$

With some suitable parameters, this circuit can exhibit chaotic oscillations. Table 1 gives the selected circuit element parameter values: the capacitance values (10 or 20 nF), the resistance values (4, 10, 25, or 45 kΩ), and the negative conductance value (− 0.0677 S), which are easily gained in the laboratory. The initial values of four state variables are assigned as $u_1(0) = 0.001$ V, $u_2(0) = 0$ V, $u_3(0) = 0$ V, and $\varphi(0) = 0$ Wb. The phase locus of the physical SBT memristor-based Wien-bridge circuit is simulated numerically, and the projections of the phase portraits onto the two-dimensional planes are shown in Fig. 2. The finite-time local Lyapunov exponents on the time interval $t \in [0, 2]$ are shown in Fig. 3, and they are calculated as $\mathrm{LE}_1 = 12.9955$, $\mathrm{LE}_2 = -4.4780$, $\mathrm{LE}_3 = -102.0071$ and $\mathrm{LE}_4 = -2829.3563$, which indicate that the physical SBT memristor-based Wien-bridge circuit is chaotic. The phase locus is a double-scroll chaotic attractor (see Fig. 2).

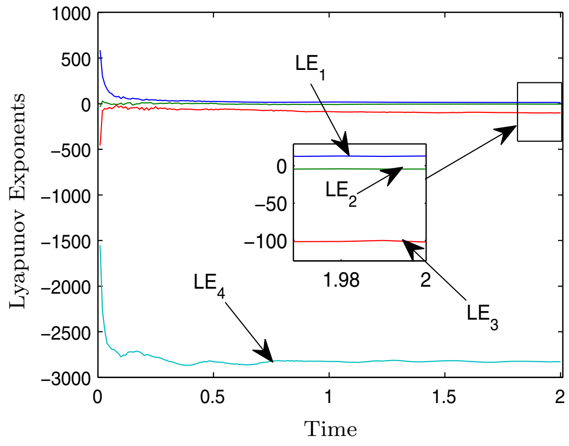

Fig. 3 The Lyapunov exponents on the time interval $t \in [0, 2]$

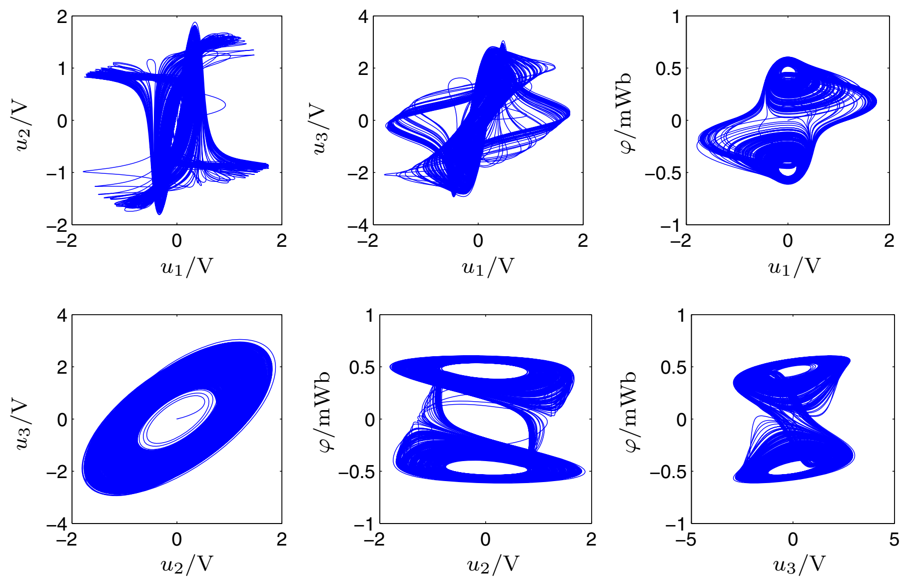

Fig. 2 The double-scroll chaotic attractor of the physical SBT memristor-based Wien-bridge circuit

3.2 Equilibrium point and stability analysis

The system is invariant when variables (u_1,u_2,u_3,φ) are transformed into ($-u_1$,$-u_2$,$-u_3$,$-\varphi$) for the state equations (1). Therefore, the SBT memristor-based Wien-bridge circuit system is symmetrical with respect to the origin. Let the right hand of state equations (1) be equal to 0. An equilibrium point is obtained as:

$$E = \{(u_1, u_2, u_3, \varphi)|u_1 = u_2 = u_3 = 0, \varphi = \varphi_0\}$$

where φ_0 is an arbitrary constant. All the points in the φ axis are equilibrium points of the fourth-order nonlinear system.

The Jacobi matrix at the equilibrium point (0, 0, 0, φ_0) can be expressed as:

$$J = \begin{bmatrix} -\frac{1}{C_1}\left(A + B|\varphi_0| + G + \frac{1}{R_5}\right) & \frac{1}{C_1 R_5} & 0 & 0 \\ \frac{1}{C_2 R_5} & \frac{1}{C_2}\left(\frac{R_4}{R_2 R_3} - \frac{1}{R_1} - \frac{1}{R_5}\right) & -\frac{1}{C_2 R_2} & 0 \\ 0 & \frac{R_4}{C_3 R_2 R_3} & -\frac{1}{C_3 R_2} & 0 \\ 1 & 0 & 0 & 0 \end{bmatrix}$$

The characteristic equation of Jacobi matrix J is as follows:

$$det(\lambda I - J) = \lambda(\lambda^3 + a_2\lambda^2 + a_1\lambda + a_0) = 0\,. \quad (2)$$

Setting the circuit element parameter values as shown in Table 1, the coefficients of characteristic equation are shown as:

$$a_2 = 0.3682|\varphi_0| \times 10^8 - 0.7667 \times 10^4,$$
$$a_1 = 4.0911|\varphi_0| \times 10^9 + 0.2889 \times 10^7,$$
$$a_0 = 2.2910|\varphi_0| \times 10^{14} - 5.3333 \times 10^{10}.$$

Equation (2) indicates that the characteristic equation of Jacobi matrix J has one zero eigenvalue and three nonzero eigenvalues. According to the Routh–Hurwitz criterion of stability, all the nonzero eigenvalues of Eq. (2) have negative real parts when $a_2 > 0$, $a_0 > 0$ and $a_2 a_1 - a_0 > 0$, namely:

$$\begin{cases} a_2 = 0.3682|\varphi_0| \times 10^8 - 0.7667 \times 10^4 > 0 \\ a_1 a_2 - a_0 = 1.5063|\varphi_0|^2 \times 10^{17} - 1.5410|\varphi_0| \times 10^{14} + 3.1185 \times 10^{10} > 0 \\ a_0 = 2.2910|\varphi_0| \times 10^{14} - 5.3333 \times 10^{10} > 0 \end{cases}$$

The solutions of inequality group are 0.2328 mWb < $|\varphi_0|$ < 0.2778 mWb or $|\varphi_0|$ > 0.7452 mWb. On the contrary, when 0 mWb < $|\varphi_0|$ < 0.2328 mWb or 0.2778 mWb < $|\varphi_0|$ < 0.7452 mWb, the equilibrium point is unstable. The system in the neighborhood of the equilibrium point may give rise to a variety of trajectories, such as stable point, period or chaos. The three nonzero eigenvalues of Jacobi matrix J are listed in Table 2 with different $|\varphi_0|$ values. The results show that the type of equilibrium point with different $|\varphi_0|$ values converts among unstable saddle-focus and stable focus.

Table 2 The three nonzero eigenvalues of Jacobi matrix with different $|\varphi_0|$ values

$\|\varphi_0\|$/mWb	λ_1	$\lambda_{2,3}$
0	8119.8070	$-226.5701 \pm 2552.8350i$
0.1	4672.3812	$-343.8573 \pm 2528.4436i$
0.2328	0	$-452.3810 \pm 1906.9927i$
0.25	−1140.1385	$-199.0974 \pm 1848.7914i$
0.2778	−2562.7270	$\pm 2006.3619i$
0.5	−10,810.6980	$33.6823 \pm 2379.4052i$
0.7452	−19,770.6063	$\pm 2436.6934i$
1	−29,120.9110	$-16.2112 \pm 2456.7393i$

3.3 Dynamic analysis of dependence on the initial state $\varphi(0)$ of the SBT memristor

The selected circuit element parameters are shown as in Table 1, the initial state values except $\varphi(0)$ are set as $u_1(0) = 0.001$ V, $u_2(0) = 0$ V, and $u_3(0) = 0$ V. The variation range of $\varphi(0)$ is from −1 to 1 mWb. When the initial state $\varphi(0)$ gradually increases, the Lyapunov exponents spectrum and the bifurcation diagram of the state variable u_1 are displayed in Fig. 4a, b, respectively.

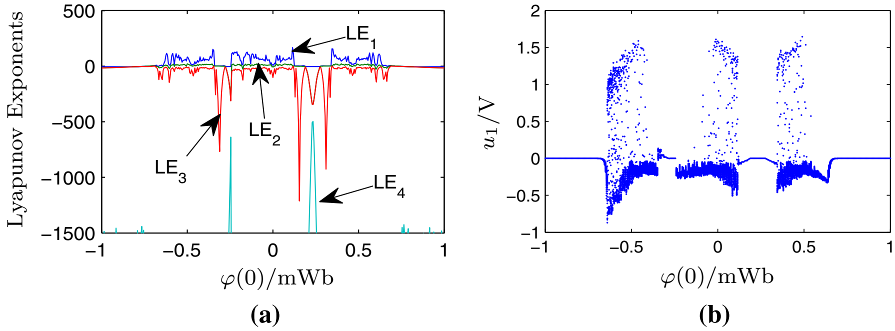

Fig. 4 Dynamic behaviors with the variation in initial state $\varphi(0)$ of the SBT memristor: **a** Lyapunov exponents spectrum, and **b** bifurcation diagram

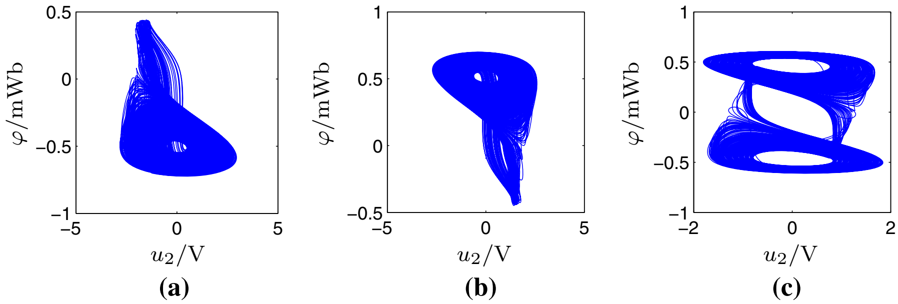

Fig. 5 The phase portraits on the $u_2-\varphi$ plane with different initial state $\varphi(0)$ value: **a** $\varphi(0) = -0.55$ mWb, **b** $\varphi(0) = -0.1$ mWb, and **c** $\varphi(0) = 0.45$ mWb

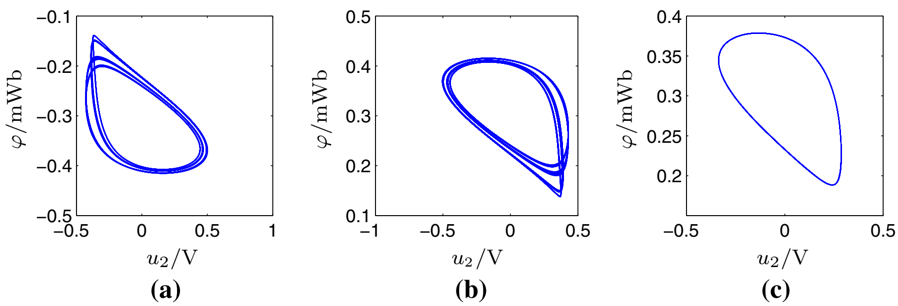

Fig. 6 The phase portraits on the $u_2 - \varphi$ plane with different initial state $\varphi(0)$ value: **a** $\varphi(0) = -0.335$ mWb, **b** $\varphi(0) = 0.13$ mWb, and **c** $\varphi(0) = 0.32$ mWb

A part of the minimum Lyapunov exponent is depicted in Fig. 4a for clarity. The bifurcation diagram coincides with Lyapunov exponents spectrum well. Figure 4 shows that the physical SBT memristor-based Wien-bridge circuit system can exhibit multiple dynamical behaviors with the variation in initial state $\varphi(0)$.

If the initial state $\varphi(0)$ is in the range of $[-1, -0.75$ mWb$]$, $[-0.28, -0.25$ mWb$]$, $[0.19, 0.28$ mWb$]$ or $[0.75, 1$ mWb$]$, the four Lyapunov exponents are less than zero and the dynamic behaviors of system can be stabilized finally (see Fig. 4).

If $\varphi(0)$ is in the range of $[-0.74, -0.35$ mWb$]$, $[-0.24, 0.11$ mWb$]$ or $[0.35, 0.74$ mWb$]$, there are positive Lynpunov exponents, and the sum of four Lyapunov exponents is negative, so the physical SBT memristor-based Wien-bridge circuit system is chaotic (see Fig. 4). For $\varphi(0) = -0.55, -0.1$ and 0.45 mWb, the phase portraits on the u_2-φ plane are depicted in Fig. 5. The circuit system exhibits chaotic behaviors, including two single-scroll attractors (Fig. 5a, b) and one double-scroll attractor (Fig. 5c).

If $\varphi(0)$ is in the range of $[-0.34, -0.29$ mWb$]$, $[0.12, 0.18$ mWb$]$ and $[0.29, 0.34$ mWb$]$, the maximum Lyapunov exponent is zero and the system is periodic (see Fig. 4). The phase portraits on the u_2-φ plane for $\varphi(0) = -0.335$, 0.13, and 0.32 mWb are shown in Fig. 6. The circuit system is 4-periodic for $\varphi(0) = -0.335$ mWb (Fig. 6a) or 0.13 mWb (Fig. 6b) and is 1-periodic for $\varphi(0) = 0.32$ mWb (Fig. 6c).

Table 3 The Lyapunov exponents and dynamical behavior with some typical initial state φ_0 values

φ_0 (mWb)	LE_1	LE_2	LE_3	LE_4	Dynamical behavior	Depicted figures
− 0.55	100.2444	8.7327	− 11.4502	− 2671.8248	Chaos	Fig. 5a
− 0.335	3.1254	1.1648	− 257.9458	− 2900.8114	Period	Fig. 6a
− 0.10	106.8943	14.4573	− 17.7949	− 2753.0446	Chaos	Fig. 5b
0.13	2.8663	− 0.9270	− 278.2424	− 2938.0157	Period	Fig. 6b
0.32	2.5685	1.4274	− 283.9530	− 2727.8649	Period	Fig. 6c
0.45	26.2849	1.0645	− 68.8281	− 2894.9695	Chaos	Fig. 5c

Table 4 The dynamics of the circuit system with the variation in the initial state $(u_1(0), u_2(0), u_3(0))$

The initial state	Interval	Dynamics	Depicted figures
$u_1(0)$	(− 5.00, − 3.80 V)	Stable point	Fig. 7
	(− 3.79, − 0.45 V)	Single-scroll attractor	
	(− 0.44, 0.44 V)	Double-scroll attractor	
	(0.45, 3.79 V)	Single-scroll attractor	
	(3.80, 5.00 V)	Stable point	
$u_2(0)$	(− 6.00, − 4.87 V)	Limit cycle	Fig. 8
	(− 4.86, − 0.40 V)	Single-scroll attractor	
	(− 0.39, 0.39 V)	Double-scroll attractor	
	(0.40, 4.86 V)	Single-scroll attractor	
	(4.87, 6.00 V)	Limit cycle	
$u_3(0)$	(− 8.00, − 7.01 V)	Stable point	Fig. 9
	(− 7.00, − 0.77 V)	Single-scroll attractor	
	(− 0.76, 0.76 V)	Double-scroll attractor	
	(0.77, 7.00 V)	Single-scroll attractor	
	(7.01, 8.00 V)	Stable point	

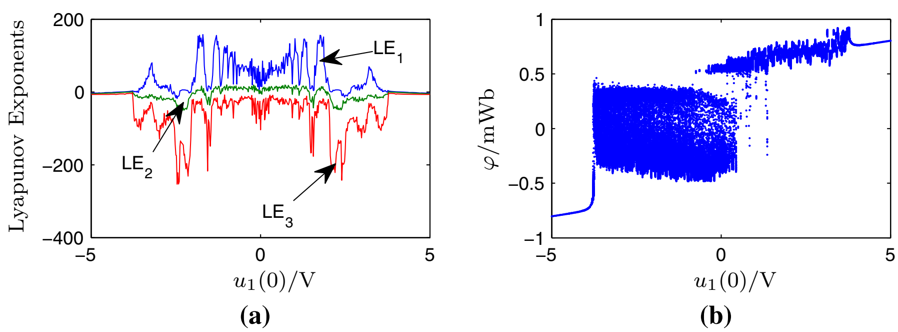

Fig. 7 Dynamic behaviors with the variation in initial state $u_1(0)$: **a** Lyapunov exponents spectrum, and **b** bifurcation diagram

The four finite-time local Lyapunov exponents on the time interval t∈[0, 2] and dynamical behavior of the circuit system with some typical initial state $\varphi(0)$ are listed in Table 3.

3.4 Dynamic analysis of dependence on other initial states

The circuit element parameters are selected as shown in Table 1. The dynamics of the circuit system with the variation in the initial state $(u_1(0), u_2(0), u_3(0))$

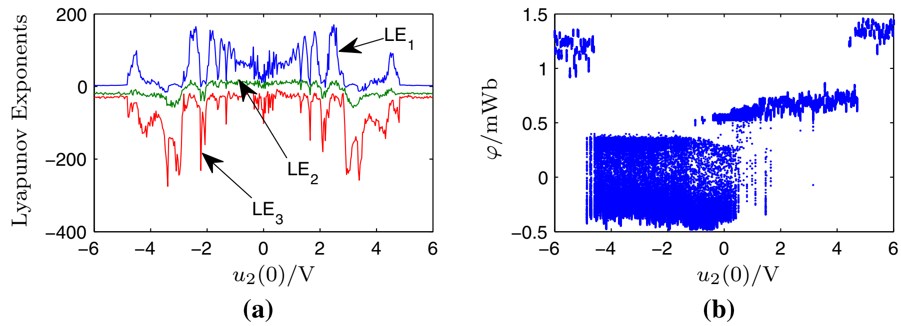

Fig. 8 Dynamic behaviors with the variation in initial state $u_2(0)$: **a** Lyapunov exponents spectrum, and **b** bifurcation diagram

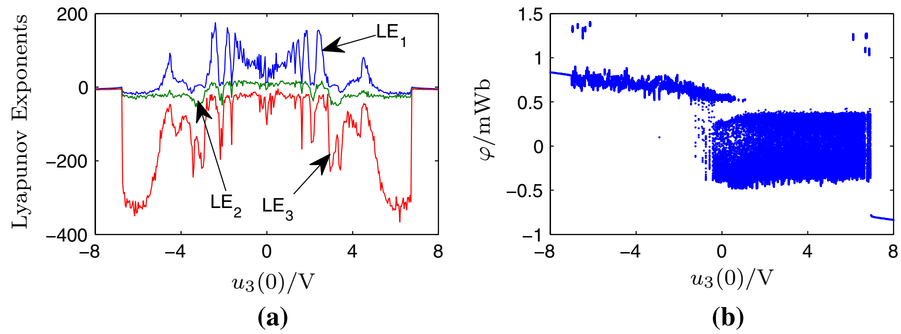

Fig. 9 Dynamic behaviors with the variation in initial state $u_3(0)$: **a** Lyapunov exponents spectrum, and **b** bifurcation diagram

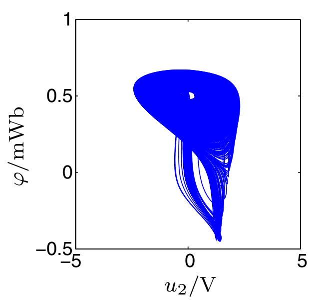

Fig. 10 A single-scroll hidden chaotic attractor at $\varphi(0) = -0.235$ mWb

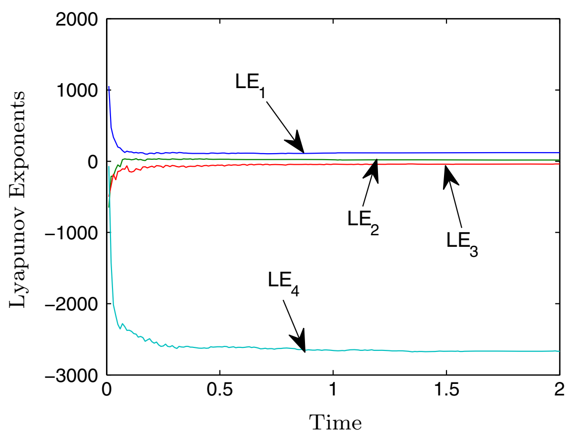

Fig. 11 The Lyapunov exponents at $\varphi(0) = -0.235$ mWb

are depicted in Table 4. The corresponding Lyapunov exponents spectrums and bifurcation diagrams are displayed in Figs. 7, 8 and 9; the minimum Lyapunov exponents are not depicted for clarity. In a word, the circuit system is very sensitive to the initial states.

3.5 A hidden chaotic attractor

The basin of a hidden attractor is not connected with equilibrium point. For example, the hidden attractors are the attractor in the system with no equilibrium point or with only one stable equilibrium point [37]. When $-0.2400\,\text{mWb} < \varphi(0) < -0.2328\,\text{mWb}$, the theoretical analysis in Sect. 3.2 shows that the equilibrium point is stable, the numerical simulation in Sect. 3.3 shows that the system is chaotic (see Fig. 4b), so the hidden attractors may exist in the system. For example, when $\varphi(0) = -0.235\,\text{mWb}$, the equilibrium point corresponding to three nonzero eigenvalues $\lambda_1 = -135.3871$ and $\lambda_{2,3} = -425.3231 \pm 1885.2675i$ is stable. By numerical simulation at $\varphi(0) = -0.235\,\text{mWb}$, the single-scroll chaotic attractor is obtained (see Fig. 10). The finite-time local

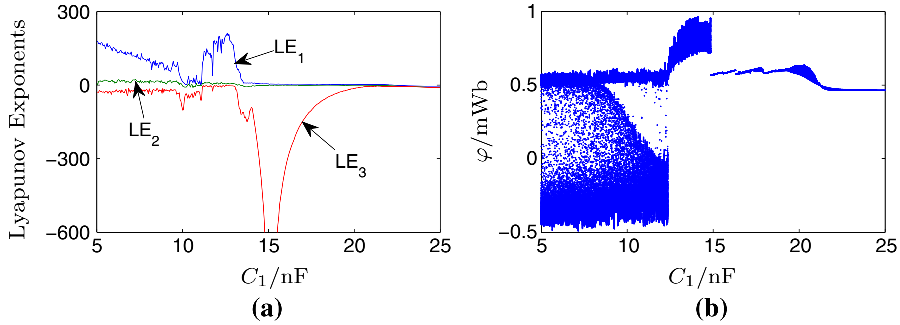

Fig. 12 Dynamic behaviors with variation in the circuit parameter C_1: **a** Lyapunov exponents spectrum, and **b** bifurcation diagram

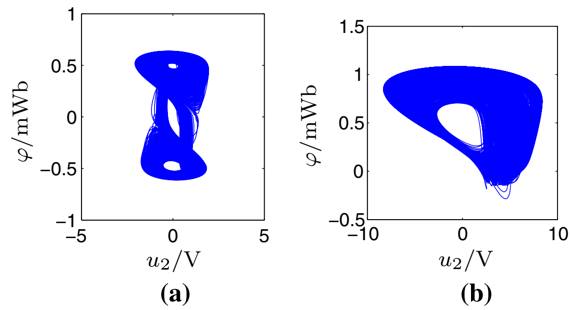

Fig. 13 The phase portraits on the u_2-φ plane with different circuit parameter C_1: **a** $C_1 = 8\,\mathrm{nF}$, and **b** $C_1 = 13\,\mathrm{nF}$

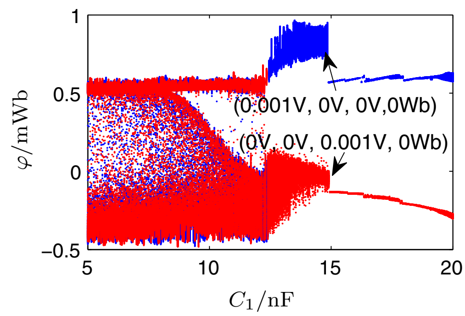

Fig. 15 Bifurcation diagram with the variation in circuit parameter C_1

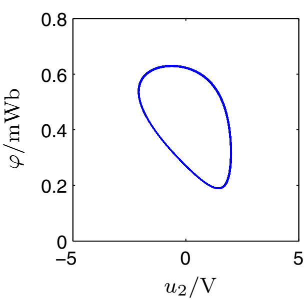

Fig. 14 The phase portraits on the u_2-φ plane for $C_1 = 18\,\mathrm{nF}$

Lyapunov exponents on the time interval t∈[0, 2] at $\varphi(0) = -0.235\,\mathrm{mWb}$ are shown in Fig. 11, and they are calculated as LE$_1$=121.5404, LE$_2$=16.5271, LE$_3 = -38.2758$ and LE$_4 = -2667.7087$, which indicates that the physical SBT memristor-based Wien-bridge circuit system is chaotic. Consequently, a hidden chaotic attractor exists in the system.

4 Dynamic analysis of dependence on circuit element parameters

4.1 Multiple dynamics with the variation in capacitance C_1

The circuit element parameters except C_1 are selected as shown in Table 1. The initial state values are set as $u_1(0) = 0.001\,\mathrm{V}$, $u_2(0) = 0\,\mathrm{V}$, $u_3(0) = 0\,\mathrm{V}$ and $\varphi(0) = 0\,\mathrm{Wb}$. The Lyapunov exponents spectrum and bifurcation diagram with the variation in C_1 are dis-

Table 5 The Lyapunov exponents and dynamical behavior with the variation in circuit parameter C_1

C_1 (nF)	LE$_1$	LE$_2$	LE$_3$	LE$_4$	Dynamical behavior	Depicted figures
8	99.5569	14.0130	−34.4005	−2681.6930	Double-scroll attractor	Fig. 13a
13	136.1033	5.3094	−4.3251	−2915.3999	Single-scroll attractor	Fig. 13b
18	3.2123	−0.4470	−70.2676	−3036.3521	Period	Fig. 14

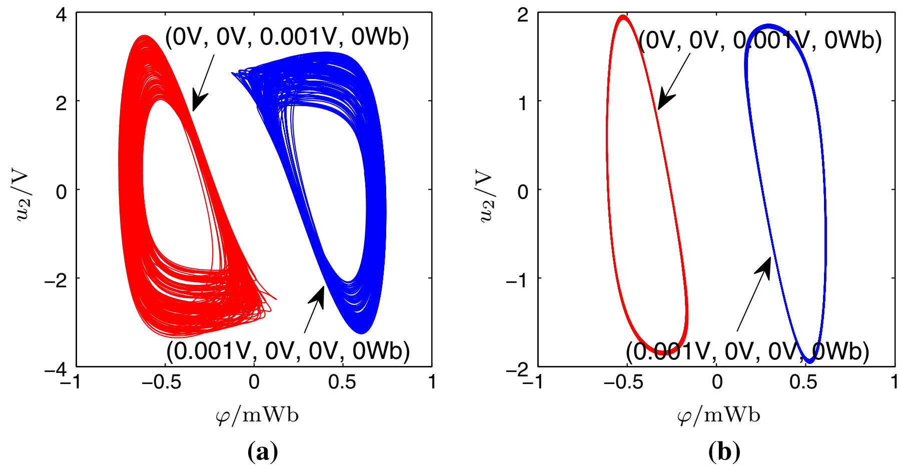

Fig. 16 The phase portraits on the φ-u_2 plane: **a** coexisting chaotic attractors at $C_1 = 13.5\,\text{nF}$, **b** coexisting periods at $C_1 = 17.0\,\text{nF}$

played in Fig. 12a, b, respectively. A part of the third Lyapunov exponent and the minimum Lyapunov exponent are not depicted in Fig. 12a for clarity. The bifurcation diagram coincides with Lyapunov exponents spectrum well.

With the increase in the capacitance C_1, the system exhibits various dynamic behaviors (see Fig. 12). If the circuit parameter C_1 is in the range of [5.0, 14.8 nF], there are positive Lynpunov exponents and the sum of four Lyapunov exponents is negative, so the physical SBT memristor-based Wien-bridge circuit system is chaotic. For $C_1 = 8$ and 13 nF, the phase portraits on the u_2-φ plane are depicted in Fig. 13. The circuit system exhibits chaotic behaviors, including a double-scroll attractor and a single-scroll attractor (see Fig. 13).

If C_1 is in the range of [14.9, 21.2 nF], the maximum Lyapunov exponent is zero, so the system is periodic. For $C_1 = 18\,\text{nF}$, the phase portrait on the u_2-φ plane is 1-periodic, as shown in Fig. 14. If C_1 is in the range of [21.3, 25.0 nF], the four Lyapunov exponents are less than zero and the locus curves converge into a stable equilibrium point.

The four finite-time local Lyapunov exponents on the time interval t∈[0, 2] and dynamical behavior of the circuit system with the variation in circuit parameter C_1 are listed in Table 5.

4.2 Coexisting chaotic attractors and coexisting periods

Selecting the circuit parameters as Table 1 except C_1, and setting the initial states as (0, 0, 0.001V, 0Wb) and (0.001, 0, 0V, 0Wb) separately, the bifurcation diagram of the state variable $\varphi(t)$ with variation of the capacitance C_1 is shown in Fig. 15. The red line is corresponding to (0, 0, 0.001 V, 0 Wb), and the blue line is corresponding to (0.001, 0, 0 V, 0 Wb) (see Fig. 15). With the two initial states, the system has coexisting chaotic attractors when C_1 is at the range of [12.5, 14.8 nF] and has coexisting periods when C_1 is at the range of [14.9, 20.0 nF]. For $C_1 = 13.5$ and 17.0 nF, the phase portraits on the φ-u_2 plane are coexisting chaotic attractors and coexisting periods with the two initial states of (0, 0, 0.001 V, 0 Wb) and (0.001, 0, 0 V, 0 Wb), as shown in Fig. 16a, b.

4.3 Dynamic analysis of dependence on other circuit element parameters

The circuit element parameters are selected as shown in Table 1. The dynamics of the circuit system with the variation in other circuit element parameters (C_2, C_3, R_1, R_2, $\frac{R_4}{R_3}$, R_5) are depicted in Table 6. The corresponding Lyapunov exponents spectrum and bifurcation diagram are displayed in Figs. 17, 18, 19, 20, 21 and 22; the minimum Lyapunov exponents are not depicted for clarity. In a word, the circuit system exhibits multiple dynamics with the variation in circuit element parameters.

5 Conclusion

In the paper, the physical SBT memristor-based Wien-bridge circuit is proposed, and its mathematical model

Table 6 The dynamics of the system with the variation in circuit element parameters (C_2, C_3, R_1, R_2, $\frac{R_4}{R_3}$, R_5)

The initial state	Interval	Dynamics	Depicted figures
C_2	(19.00, 20.54 nF)	Chaos	Fig. 17
	(20.55, 20.85 nF)	Period	
	(20.86, 21.00 nF)	Stable point	
C_3	(19.00, 19.20 nF)	Stable point	Fig. 18
	(19.21, 19.51 nF)	Period	
	(19.52, 21.00 nF)	Chaos	
R_1	(23.50, 23.97 kΩ)	Stable point	Fig. 19
	(23.98, 24.45 kΩ)	Period	
	(24.46, 27.00 kΩ)	Chaos	
R_2	(23.50, 25.41 kΩ)	Chaos	Fig. 20
	(25.42, 25.75 kΩ)	Period	
	(25.76, 26.00 kΩ)	Stable point	
$\frac{R_4}{R_3}$	(2.400, 2.458)	Stable point	Fig. 21
	(2.459, 2.477)	Period	
	(2.478, 2.550)	Chaos	
R_5	(35.00, 40.09 kΩ)	Stable point	Fig. 22
	(40.10, 42.20 kΩ)	Period	
	(42.21, 50.00 kΩ)	Chaos	

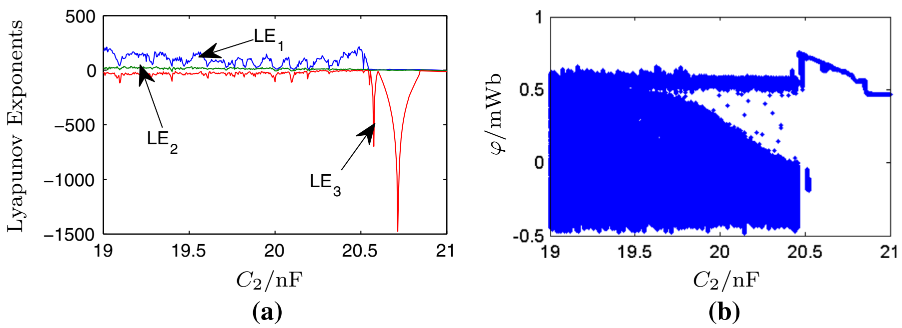

Fig. 17 Dynamic behaviors with the variation in circuit parameter C_2: **a** Lyapunov exponents spectrum, and **b** bifurcation diagram

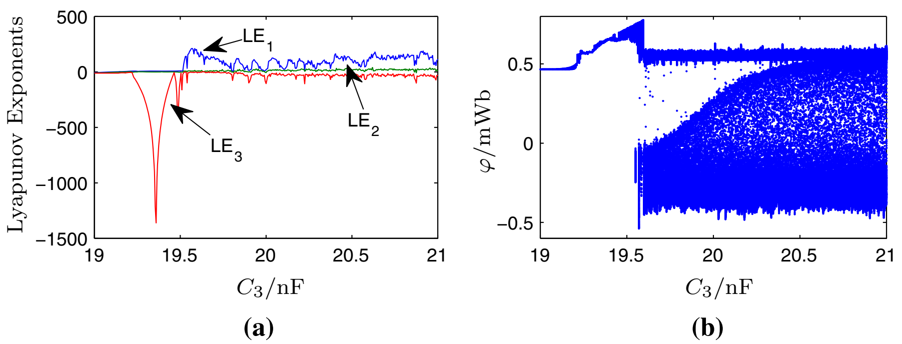

Fig. 18 Dynamic behaviors with the variation in circuit parameter C_3: **a** Lyapunov exponents spectrum, and **b** bifurcation diagram

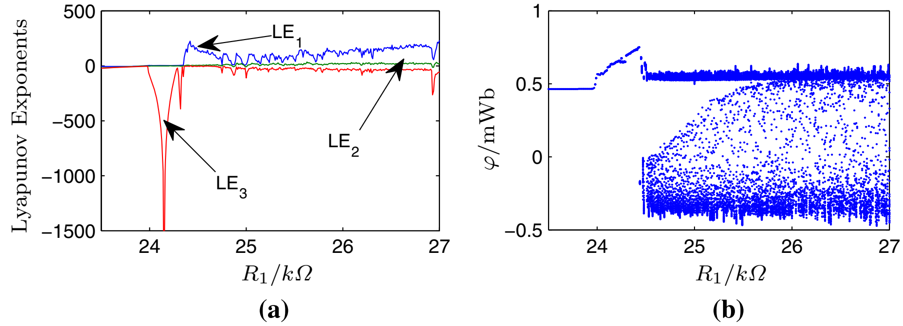

Fig. 19 Dynamic behaviors with the variation in circuit parameter R_1: **a** Lyapunov exponents spectrum, and **b** bifurcation diagram

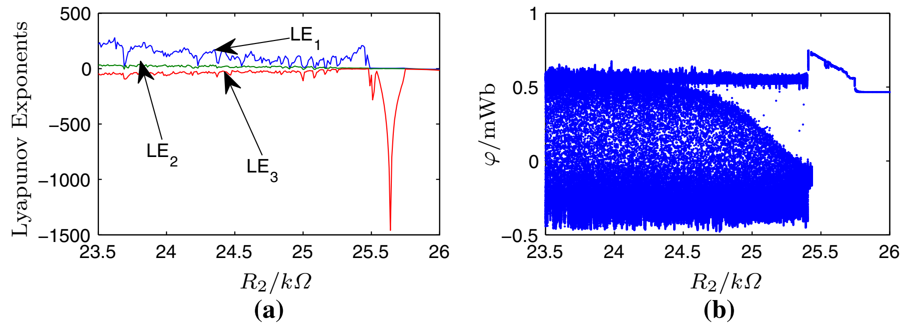

Fig. 20 Dynamic behaviors with the variation in circuit parameter R_2: **a** Lyapunov exponents spectrum, and **b** bifurcation diagram

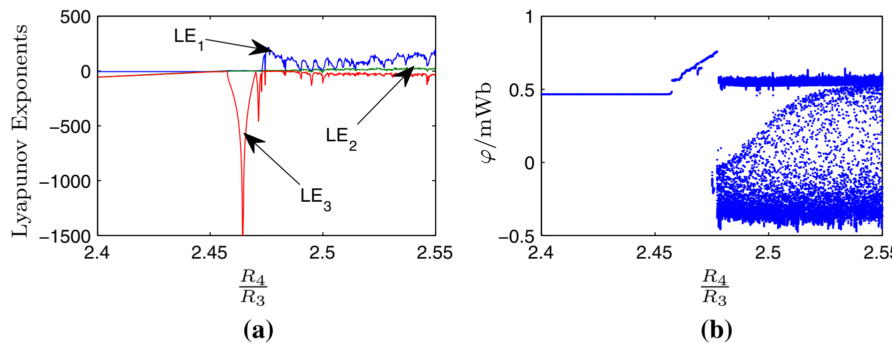

Fig. 21 Dynamic behaviors with the variation in circuit parameter $\frac{R_4}{R_3}$: **a** Lyapunov exponents spectrum, and **b** bifurcation diagram

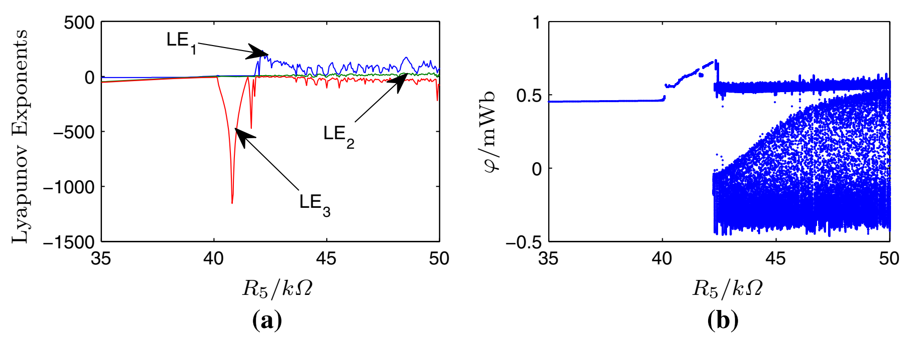

Fig. 22 Dynamic behaviors with the variation in circuit parameter R_5: **a** Lyapunov exponents spectrum, and **b** bifurcation diagram

is established using fourth-order state equations. The system generates typical chaotic attractors by choosing suitable circuit element parameters. By means of theoretical analysis, when $0.2328\,\mathrm{mWb} < |\varphi_0| < 0.2778\,\mathrm{mWb}$ or $|\varphi_0| > 0.7452\,\mathrm{mWb}$, the equilibrium point is stable; when $0\,\mathrm{mWb} < |\varphi_0| < 0.2328\,\mathrm{mWb}$ and $0.2778\,\mathrm{mWb} < |\varphi_0| < 0.7452\,\mathrm{mWb}$, the equilibrium point is unstable. Moreover, the numerical simulation results indicate that this circuit system exhibits various dynamic behaviors with the variation in the initial states and the circuit element parameters. Specifically, some interesting dynamic behaviors have been found. When the initial state $\varphi(0)$ is in the range of $[-0.2400, -0.2328\,\mathrm{mWb}]$, the system can generate hidden chaotic attractors. When the capacitance C_1 is in the range of [12.5, 20.0 nF], the system can generate coexisting chaotic attractors and coexisting periods. All the results provide an important theoretical basis for the next physical implementation of the chaotic circuit.

Acknowledgements We appreciate editor and reviewers for their helpful and constructive comments on our manuscript. Some pieces of comments even enlighten us for future researches. We appreciate Dr. Fang Yuan for valuable discussion. This work was supported by the National Natural Science Foundation of China (Nos. 61703247, 61703246, 61473177) the China Postdoctoral Science Foundation (No. 2015M582114), the Shandong Postdoctoral Special Foundation (No. 201502017),and the Qingdao Science and Technology Plan Project(No. 15-9-1-39-jch).

References

1. Kia, B., Mobley, K., Ditto, W.L.: An integrated circuit design for a dynamics-based reconfigurable logic block. IEEE Trans. Circuits II **PP(99)**, 1-1 (2016)
2. https://news.ncsu.edu/2016/09/kia-mooreslaw/. Accessed 20 Sep 2016
3. Chua, L.: Memristor-the missing circuit element. IEEE Trans. Circuit Theory **18**, 507–519 (1971)
4. Itoh, M., Chua, L.O.: Memristor cellular automata and memristor discrete-time cellular neural networks. Int. J. Bifurc. Chaos **19**, 3605–3656 (2009)
5. Muthuswamy, B.: Implementing memristor based chaotic circuits. Int. J. Bifurc. Chaos **20**, 1335–1350 (2010)
6. Peng, G., Min, F.: Multistability analysis, circuit implementations and application in image encryption of a novel memristive chaotic circuit. Nonlinear Dyn. **90**(3), 1607–1625 (2017)
7. Wang, C., Liu, X., Xia, H.: Multi-piecewise quadratic nonlinearity memristor and its 2N-scroll and 2N+1-scroll chaotic attractors system. Chaos **27**, 033114 (2017)
8. Kim, B.K., Nguyen, V.H., Kim, N.T., et al.: Experimental study on chaotic behaviors of a Chuas circuit based on variable memristor. IEICE Electron. Expr. **12**, 20150457 (2015)
9. Li, Y., Huang, X., Guo, M.: The generation, analysis, and circuit implementation of a new memristor based chaotic system. Math. Probl. Eng. **2013**, 398306 (2013)
10. Ma, J., Chen, Z., Wang, Z., et al.: A four-wing hyper-chaotic attractor generated from a 4-D memristive system with a line equilibrium. Nonlinear Dyn. **81**(3), 1275–1288 (2015)
11. Wen, S., Huang, T., Yu, X., et al.: Sliding-mode control of memristive Chua's systems via the event-based method. IEEE Trans. Circuits II **64**(1), 81–85 (2017)
12. Zhou, L., Wang, C., Zhou, L.: Generating hyperchaotic multi-wing attractor in a 4D memristive circuit. Nonlinear Dyn. **85**, 2653–2663 (2016)
13. Danca, M.F., Tang, W.K.S., Chen, G.: Suppressing chaos in a simplest autonomous memristor-based circuit of fractional order by periodic impulses. Chaos Solitons Fractals **84**, 31–40 (2016)
14. Chen, Q., Wang, X., Wan, H., et al.: A circuit design for multi-inputs stateful OR gate. Phys. Lett. A **380**, 3081–3085 (2016)
15. Dadras, S., Momeni, H.R.: A novel three-dimensional autonomous chaotic system generating two, three and four-scroll attractors. Phys. Lett. A **373**(40), 3637–3642 (2009)
16. Kengne, J., Njitacke, T.Z., Kamdoum, T.V., et al.: Periodicity, chaos, and multiple attractors in a memristor-based Shinriki's circuit. Chaos **25**(10), 103126 (2015)
17. Dadras, S., Momeni, H.R.: Four-scroll hyperchaos and four-scroll chaos evolved from a novel 4D nonlinear smooth autonomous system. Phys. Lett. A **374**(11), 1368–1373 (2010)
18. Strukov, D.B., Snider, G.S., Stewart, D.R., Williams, R.S.: The missing memristor found. Nature **453**, 80–83 (2008)
19. Ren, G., Zhou, P., Ma, J., et al.: Dynamical response of electrical activities in digital neuron circuit driven by autapse. Int. J. Bifurc. Chaos **27**(12), 1750187 (2017)
20. Ren, G., Xu, Y., Wang, C.: Synchronization behavior of coupled neuron circuits composed of memristors. Nonlinear Dyn. **88**(2), 893–901 (2017)
21. Zhang, G., Ma, J., Alsaedi, A., et al.: Dynamical behavior and application in Josephson junction coupled by memristor. Appl. Math. Comput. **321**, 290–299 (2018)
22. Xu, Y., Jia, Y., Ma, J., et al.: Synchronization between neurons coupled by memristor. Chaos Solitons Fractals **104**, 435–442 (2017)
23. Wu, F., Wang, C., Jin, W., Ma, J.: Dynamical responses in a new neuron model subjected to electromagnetic induction and phase noise. Physica A **469**, 81–88 (2017)
24. Wen, S., Zeng, Z., Huang, T., et al.: Exponential adaptive lag synchronization of memristive neural networks via fuzzy method and applications in pseudorandom number generators. IEEE Trans. Fuzzy Syst. **22**(6), 1704–1713 (2014)
25. Driscoll, T., Kim, H.T., Chae, B.G., et al.: Phase-transition driven memristive system. Appl. Phys. Lett. **95**, 043503 (2009)
26. Hasegawa, T., Ohno, T., Terabe, K., et al.: Learning abilities achieved by a single solid-state atomic switch. Adv. Mater. **22**, 1831–1834 (2010)
27. Chang, T., Jo, S.H., Kim, K.H., et al.: Synaptic behaviors and modeling of a metal oxide memristive device. Appl. Phys. A Mater. **102**, 857–863 (2011)
28. Wang, Z.Q., Xu, H.Y., Li, X.H., Yu, H., Liu, Y.C., Zhu, X.J.: Synaptic learning and memory functions achieved using

oxygen ion migration/diffusion in an amorphous InGaZnO memristor. Adv. Funct. Mater. **22**(13), 2759–2765 (2012)
29. Li, Y., Zhong, Y., Xu, L., Zhang, J., Xu, X., Sun, H., Miao, X.: Ultrafast synaptic events in a chalcogenide memristor. Sci. Rep. **3**, 1619 (2013)
30. Li, Y.X., Dou, G.: Towards the implementation of memristor: a study of the electric properties of $Ba_{0.77}Sr_{0.23}TiO_3$ material. Int. J. Bifurc. Chaos **23**(12), 1350204 (2013)
31. Wang, Z., Joshi, S., Savelev, S.E., et al.: Memristors with diffusive dynamics as synaptic emulators for neuromorphic computing. Nat. Mater. **16**, 101–108 (2017)
32. Dou, G., Yu, Y., Guo, M., et al.: Memristive behavior based on Ba-doped $SrTiO_3$ films. Chin. Phys. Lett. **34**, 038502 (2017)
33. Zhang, Y.M., Dou, G., Sun, Z., Guo, M., Li, Y.X.: Establishment of physical and mathematical models for $Sr_{0.95}Ba_{0.05}TiO_3$ memristor. Int. J. Bifurc. Chaos **27**(9), 1750148 (2017)
34. Kuznetsov, N.V., Leonov, G.A., Mokaev, T.N., et al.: Finite-time Lyapunov dimension and hidden attractor of the Rabinovich system. Nonlinear Dyn. (2018). https://doi.org/10.1007/s11071-018-4054-z
35. Kuznetsov, N.V., Alexeeva, T.A., Leonov, G.A.: Invariance of Lyapunov exponents and Lyapunov dimension for regular and irregular linearizations. Nonlinear Dyn. **85**(1), 195–201 (2016)
36. Leonov, G.A., Kuznetsov, N.V.: Time-varying linearization and the Perron effects. Int. J. Bifurc. Chaos **17**(4), 1079–1107 (2007)
37. Leonov, G.A., Kuznetsov, N.V., Mokaev, T.N.: Hidden attractor and homoclinic orbit in Lorenz-like system describing convective fluid motion in rotating cavity. Commun. Nonlinear Sci. **28**, 166–174 (2015)